TMEM55B controls lipolysis via lysosomal pH and ER–lysosome calcium signaling

Nagi Mukae[1], Honoka Maki[1] & Michiko Shirane[1]*

[1]Department of Molecular Biology, Graduate School of Pharmaceutical Sciences, Nagoya City University, Nagoya, Aichi, Japan.

*Corresponding: M.S. (shiram@phar.nagoya-cu.ac.jp)

Keywords:
TMEM55B, PDZD8, Lysosomes, Endoplasmic reticulum, Calcium, Membrane contact sites

ABSTRACT

A cholesterol transfer protein PDZD8 promotes lipolysis by facilitating endosomal maturation through membrane contact sites (MCSs) between endoplasmic reticulum (ER) and endolysosomes (LE/Ly). Endosomal maturation are suggested to be associated with endosomal acidification and calcium dynamics. However, the detailed mechanism by which the ER protein PDZD8 promotes endosomal maturation remained unclear. Here, we identified TMEM55B as a PDZD8-binding protein that localizes to lysosomes and is involved in cholesterol metabolism. TMEM55B functions as a regulator of the v-ATPase complex. Suppression of TMEM55B expression reduced lysosomal acidification, leading to impaired lipid droplet degradation, as well as decreased lysosomal calcium release and uptake, which in turn diminished calcium-induced calcium release (CICR) at ER–LE/Ly MCSs. These findings indicate that the lysosomal protein TMEM55B regulates lysosomal acidification and calcium dynamics through its interaction with the ER protein PDZD8, thereby promoting endosomal maturation and lipid metabolism.

Introduction

ER- LE/Ly MCSs are not formed by random contacts between the ER and endosomes but are mediated by specific membrane tethering complexes. ORP1L and VAP were first identified as tethering factors of ER–LE/Ly MCSs, and subsequent studies revealed that many sterol transfer proteins—including ORP, STARD, and Lam families, as well as NPC1, Protrudin, and PDZD8—also function at these sites[1-3]. The tethering of ER–LE/Ly MCSs is strengthened during endosomal maturation, a process involving both endosomal acidification and Ca^{2+} dynamics. Cholesterol and Ca^{2+} therefore serve as key messengers mediating cross-talk between these two organelles at ER–LE/Ly MCSs[4].

Cells acquire cholesterol through two main pathways: de novo synthesis and endocytosis of lipoproteins (LPs)[5-7]. In the brain, however, neurons lack the ability to synthesize cholesterol and instead rely on supply from glial cells. Cholesterol produced in glia is esterified to cholesteryl esters (CEs), packed into HDL-like lipoproteins, transported to neurons, internalized via LDLR-mediated endocytosis, and hydrolyzed to free cholesterol by lysosomal acidic lipases[7,8]. This cholesterol is then trafficked to the ER and redistributed to other organelles for cellular functions[4,9].

CEs stored in lipid droplets (LDs) are degraded through lipophagy, a form of microautophagy in which LDs fuse with lysosomes, enabling lipids to be hydrolyzed by lysosomal acidic lipases[10-13]. Endocytosed LP particles are degraded in a similar manner.

Thus, endosomal maturation, which depends on lysosomal acidification, is essential for metabolizing CEs from both LDs and LPs into cholesterol.

PDZD8 is an ER membrane protein originally identified as a Protrudin-binding partner, with both proteins acting as tethers at ER–LE/Ly MCSs[14-20]. PDZD8 belongs to the TULIP super family and mediates cholesterol transport through its SMP domain[16,21,22]. Because Protrudin interacts with VAP via its FFAT motif, the PDZD8–Protrudin–VAP complex is thought to function in lipid transport[3]. PDZD8 thereby contributes to cholesterol metabolism by promoting lipolysis through endosomal maturation in neurons[23]. Consistently, PDZD8-deficient mice exhibit CE accumulation in the brain due to impaired lipolysis, along with memory and emotional dysfunction[24,25]. CE accumulation is also observed in the brains of Alzheimer's disease (AD) patients and AD model mice[26-28]. In particular, neurons carrying the APOE4 allele—the strongest genetic risk factor for AD—show CE accumulation with lipofuscin formation due to impaired lysosomal function[29,30].

Compared with cholesterol metabolism, research on lysosomal calcium dynamics is relatively recent, and many questions remain unresolved. As endosomes undergo luminal acidification, their Ca^{2+} concentration increases, and lysosomes eventually become a major intracellular Ca^{2+} store alongside the ER and mitochondria. Ca^{2+} uptake into the endosomal lumen promotes intraluminal vesicle fusion, thereby facilitating endosomal maturation[31-34]. Conversely, calcium-induced calcium release (CICR)—in which a small amount of Ca^{2+} efflux from lysosomes trigger large scale release from the ER IP_3 receptors and ryanodine receptors—has emerged as an important mechanism of transient Ca^{2+} signaling[35-39]. Endosomal acidification activates lysosomal Ca^{2+} channels, such as two-pore channel-2 (TPC2) and TRPML1, which promote Ca^{2+} release from lysosomes. Although Ca^{2+} dynamics at ER–LE/Ly MCSs have been implicated in diverse cellular processes[34,40], their detailed mechanisms remain poorly understood.

TMEM55B has been reported to perform multiple functions. It was first identified as a phosphatase that hydrolyzes the 4-position phosphate of PtdIns(4,5)P_2 to generate PtdIns(5)P[41,42]. TMEM55B is a lysosomal membrane protein that interacts with the v-ATPase and Ragulator complexes, thereby contributing to v-ATPase activation and subsequent mTORC1 signaling at the lysosomal membrane[43]. Consistent with its importance, TMEM55B knockout mice are embryonic lethal[43]. Because v-ATPase is a proton pump essential for endolysosomal acidification, its dysfunction leads to various lysosomal storage diseases[44-46]. TMEM55B also cooperates with TFEB and JIP4 to promote dynein-dependent retrograde lysosomal transport[47] and participate in lysosomal

88 oxidative stress responses[48]. In addition, TMEM55B regulates the expression and activity
89 of LDLR thereby modulating lipoprotein uptake and cholesterol metabolism[49,50].
90 In this study, we identified TMEM55B as a PDZD8-interacting lysosomal protein that
91 regulates cholesterol metabolism via lysosomal acidification and Ca^{2+} dynamics at ER–
92 LE/Ly MCSs.
93
94 **Results**
95 **PDZD8 interacts with the lysosomal protein TMEM55B.**
96 In neuronal cells, the lipid transfer protein PDZD8 promotes cholesterol metabolism via
97 endosomal maturation; however, the mechanism by which this ER protein regulates
98 lysosomal activity remains unclear. To identify lysosomal proteins interacting with
99 PDZD8, we established a Neuro2A cell line stably expressing 3×FLAG-tagged PDZD8.
100 The PDZD8 complex was isolated by anti-FLAG immunoprecipitation, separated by
101 SDS-PAGE, digested with trypsin, and analyzed by LC-MS/MS. In parallel, the same
102 analysis was performed using cells transfected with empty vector to exclude nonspecific
103 binding. Proteins reproducibly detected across three independent experiments were
104 extracted, and semiquantitative analysis based on identification frequency (IF)[51]
105 identified 196 proteins with IF > 0.01. Among those, 13 endosome-localized proteins
106 were selected using GO Term and UniProt subcellular localization annotations (Fig. 1A).
107 This group included the lysosomal protein TMEM55B and its binding partners, v-ATPase
108 subunit Atp6v0d1 and Lamtor1 (Fig. 1A)[43]. Notably, Lamtor1 and TMEM55B are
109 lysosome-localized proteins associated with cholesterol metabolism, suggesting a
110 potential role in lipolysis-mediated cholesterol processing. Since TMEM55B regulates
111 the v-ATPase complex, we focused on TMEM55B as a possible upstream regulator of
112 PDZD8-mediated lysosomal function.
113
114 **TMEM55B is not essential for ER–LE/Ly tethering.**
115 Because PDZD8 functions as a tether at ER–LE/Ly MCSs, we examined whether its
116 binding partner TMEM55B also contributes to this process. TMEM55B expression was
117 suppressed in HeLa cells using siRNA (siTMEM55B), resulting in a marked reduction of
118 both RNA and protein levels compared with control cells (siControl) (Fig. 1B, C). To
119 assess ER–LE/Ly contacts, we employed a split-GFP system in which GFP fluorescence
120 is reconstituted only when ER and lysosomal membranes are closely apposed[16,52]. Cells
121 were co-transfected with ERj1-GFP(1–10) (ER-localized fragment) and LAMP1-
122 GFP(11) (lysosomal fragment), together with mCherry to normalize expression levels.
123 The GFP/mCherry fluorescence ratio per cell, reflecting ER–LE/Ly MCS formation, was

124 quantified (Fig. 1D). No significant difference in GFP/mCherry ratio was observed
125 between siTMEM55B and siControl cells (Fig. 1E). These results demonstrate that,
126 unlike PDZD8, TMEM55B is not required for tethering of ER–LE/Ly MCSs.
127
128 **TMEM55B regulates lysosomal acidification and activity.**
129 TMEM55B interacts with the v-ATPase complex and has been implicated in its regulation.
130 We therefore hypothesized that TMEM55B contributes to lysosomal acidification and
131 activity via v-ATPase. To test this, HeLa cells transfected with siControl or siTMEM55B
132 were stained with LysoTracker (Fig. 2A) or LysoSensor (Fig. 2C), both of which increase
133 in fluorescence intensity as lysosomal pH decreases. In both assays, siTMEM55B cells
134 showed significantly reduced fluorescence compared with controls, indicating impaired
135 lysosomal acidification (Fig. 2B, D). To assess the functional consequences in neurons,
136 we suppressed TMEM55B expression in PC12 cells (Fig. 2E) and evaluated lipolysis
137 using EGFP-PLIN2 as a lipid droplet (LD) marker and LysoTracker Red as a lysosomal
138 marker (Fig. 2F). TMEM55B knockdown cells exhibited enlarged LDs (Fig. 2G) with
139 increased LD fluorescence intensity per cell (Fig. 2H), as well as reduced LysoTracker
140 fluorescence (Fig. 2I), consistent with defective lysosomal acidification and impaired
141 lipolysis. Furthermore, LD–lysosome fusion events were significantly decreased in
142 siTMEM55B cells compared with controls (Fig. 2J). Together, these results demonstrate
143 that TMEM55B promotes lysosomal acidification and activity, thereby facilitating LD
144 degradation and lipolysis.
145
146 **TMEM55B promotes Ca^{2+} release from the ER.**
147 Intracellular Ca^{2+} elevation promotes lysosome fusion with other organelles[44], suggesting
148 that lipolysis mediated by the PDZD8–TMEM55B complex could involve Ca^{2+} signaling
149 at ER–LE/Ly MCSs. Since the ER is the major intracellular Ca^{2+} store, we investigated
150 whether TMEM55B regulates Ca^{2+} release or uptake from the ER. HeLa cells were
151 transfected with the ER-targeted Ca^{2+} indicator G-CEPIA1er[53], which binds ER luminal
152 Ca^{2+} and emits GFP fluorescence, and colocalization with the ER marker KDEL was
153 confirmed by confocal microscopy (Fig. 3A, B). To assess ER Ca^{2+} dynamics, siControl
154 or siTMEM55B cells were stimulated with ATP to induce transient ER Ca^{2+} release,
155 followed by Ca^{2+} reuptake to the ER. In siTMEM55B cells, ATP-induced Ca^{2+} release as
156 well as reuptake were markedly reduced compared with controls (Fig. 3C, D).
157 Quantitative analysis revealed that siTMEM55B cells exhibited significantly decreased
158 rates of ER Ca^{2+} release (Fig. 3E), slower subsequent Ca^{2+} reuptake (Fig. 3F), and delayed

159 time to peak Ca^{2+} release (Fig. 3G). These findings indicate that TMEM55B facilitates
160 ATP-stimulated transient Ca^{2+} release from the ER.
161
162 **TMEM55B promotes Ca^{2+} release from lysosomes.**
163 We next investigated whether TMEM55B regulates Ca^{2+} release from lysosomes and how
164 this affects ER Ca^{2+} dynamics. Lysosomal Ca^{2+} release and uptake were monitored using
165 Ly-GG, which binds cytosolic Ca^{2+} at the lysosomal membrane and emits GFP
166 fluorescence[54] (Fig. 4A). Co-expression of Ly-GG with the lysosomal marker LAMP1
167 confirmed colocalization (Fig. 4B). ATP stimulation of siControl HeLa cells induced
168 transient Ca^{2+} release from lysosomes. In siTMEM55B cells, the magnitude (Fig. 4C) and
169 rate (Fig. 4D) of lysosomal Ca^{2+} release were significantly reduced compared to controls.
170 The subsequent Ca^{2+} reuptake rate was also decreased (Fig. 4E), indicating impaired
171 lysosomal Ca^{2+} dynamics. As a control, we examined mitochondrial Ca^{2+} using
172 CEPIA3mt[53], which binds mitochondrial matrix Ca^{2+}, together with the mitochondrial
173 marker Su9-RFP[55] (Fig. 4F), confirmed colocalization (Fig. 4G). ATP stimulation
174 induced transient mitochondrial Ca^{2+} increases as well as decrease, which were not
175 significantly different between siControl and siTMEM55B cells (Fig. 4H–J). These
176 results indicate that TMEM55B specifically regulates lysosomal Ca^{2+} dynamics without
177 affecting mitochondrial Ca^{2+}.
178
179 **Discussion**
180 Lysosomes serve as central hubs for cellular metabolism, coordinating degradation,
181 nutrient recycling, and signaling. Proper lysosomal acidification and calcium homeostasis
182 are essential for lipid metabolism and neuronal function, and their dysregulation has been
183 increasingly linked to neurodegenerative diseases. Despite this, the molecular
184 mechanisms connecting lysosomal function to lipid regulation remain incompletely
185 understood.
186 In this study, we identify TMEM55B as a key lysosomal regulator that interacts with the
187 ER protein PDZD8 to control lysosomal acidification and calcium dynamics. TMEM55B
188 promotes endosomal maturation and lipid droplet degradation, revealing a novel
189 mechanism linking lysosomal activity to lipid metabolism. These findings provide new
190 insights into cellular lipid homeostasis and suggest potential targets for disorders
191 associated with lysosomal dysfunction and cholesterol metabolism.
192 The lipid transfer protein PDZD8 mediates tethering of ER–LE/Ly membrane contact
193 sites (MCSs) and facilitates cholesterol metabolism through lipolysis via endosomal
194 maturation. However, the mechanism by which PDZD8 promotes endosome maturation

195 has remained unclear. Through complex analysis in neuronal cells, we identified Lamtor1
196 and TMEM55B as lysosome-localized, cholesterol-associated proteins among LE/Ly
197 candidates. Given that TMEM55B regulates the v-ATPase complex, we focused on its
198 intracellular functions.
199 We found that TMEM55B contributes to lysosomal acidification and activation. Loss of
200 TMEM55B impaired lysosomal Ca^{2+} release and uptake, as well as ATP-stimulated Ca^{2+}
201 release from the ER, while mitochondrial Ca^{2+} dynamics remained unaffected. In our
202 system, lysosomal Ca^{2+} release peaked within 180 s after ATP stimulation (Fig. 4C),
203 whereas ER Ca^{2+} release peaked later (Fig. 3C), consistent with calcium-induced calcium
204 release (CICR) from the ER triggered by lysosomal Ca^{2+} release. These results indicate
205 that TMEM55B promotes endosomal maturation via lysosomal acidification and
206 activation, and facilitates CICR at ER–LE/Ly MCSs, thereby supporting lipolysis (Fig.
207 5).
208 The PDZD8–TMEM55B complex thus plays a central role in ER–LE/Ly MCS functions,
209 including endosomal maturation, Ca^{2+} dynamics, and cholesterol metabolism.
210 Nevertheless, the effects of TMEM55B deficiency on lysosomal fusion and lipid droplet
211 degradation were partial, failing to recapitulate the strong phenotype observed with
212 PDZD8 deficiency. This suggests that additional, as-yet-unidentified mechanisms
213 contribute to PDZD8-mediated lipolysis.
214 In summary, TMEM55B enhances lysosomal acidification via v-ATPase regulation,
215 thereby increasing lysosomal enzyme activity and promoting lipolysis. Lysosomal
216 acidification also activates Ca^{2+} channels, facilitating CICR at ER–LE/Ly MCSs and
217 supporting cholesterol metabolism through lysosomal fusion. Direct evidence linking
218 TMEM55B-mediated CICR to enhanced lipolysis, however, remains lacking, and further
219 studies are needed to clarify this mechanism.
220
221
222 **Methods**
223 **Plasmids**
224 EGFP and mCherry vectors were from Clontech (Mountain View, CA, US). Human
225 cDNAs encoding PLIN2 (GenBank accession number NM_007408.4), LAMP1
226 (GenBank accession number BC025335), and KDEL with the signal sequence of
227 calreticulin (GenBank accession number NM_004343) were amplified from HeLa cells
228 by the polymerase chain reaction (PCR) with PrimeSTAR HS DNA polymerase (Takara,
229 Shiga, Japan). pCMV-G-CEPIA1er (Addgene plasmid #58215) and pCMV-CEPIA3mt
230 (Addgene plasmid #58219) were obtained from Addgene (Watertown, MA, US). Ly-GG

231 was kindly provided by Dr. CW Taylor (University of Cambridge, UK). Vectors for split-
232 GFP analysis, ERj1–GFP(1–10) and LAMP1–GFP(11), were kindly provided by Dr.
233 Tamura (Yamagata University, Japan). The pSu9 cDNA was kindly provided by Dr.
234 Mihara (Kyushu University, Japan). The mRFP cDNA was kindly provided by Dr. R.Y.
235 Tsien (University of California, San Diego, US).
236
237 **Antibodies**
238 Antibodies to TMEM55B were from Proteintech (Rosemont, IL, USA); antibodies to
239 HSP90 were from BD Biosciences (Franklin Lakes, NJ, USA).
240
241 **Cell culture, transfection, and retrovirus infection**
242 HeLa cells (CCL-2, purchased from ATCC, US) were cultured under a humidified
243 atmosphere of 5% CO_2 at 37°C in Dulbecco's modified Eagle's medium (Invitrogen Life
244 Technologies) supplemented with 10% fetal bovine serum (Invitrogen Life Technologies).
245 The culture medium for Plat-E cells was also supplemented with blasticidin (10 μg/ml).
246 Cells were transfected with the use of XtremeGene9 reagents (Roche Diagnostics,
247 Mannheim, Germany) according to the manufacturer's protocol. For retroviral infection,
248 Plat-E cells were transiently transfected with pMX-puro–based vectors and then cultured
249 for 48 h. The retroviruses in the resulting culture supernatants were used to infect
250 Neuro2A cells, and the cells were then subjected to selection with puromycin (1 μg/ml).
251
252 **Identification and categorization of PDZD8-associated proteins**
253 Neuro2a cells infected with a retrovirus encoding FLAG–tagged mouse PDZD8 or with
254 the corresponding empty virus were solubilized in a lysis buffer (40 mM HEPES-NaOH
255 [pH 7.5], 150 mM NaCl, 10% glycerol, 0.5% Triton X-100, 1 mM Na_3VO_4, 25 mM NaF,
256 aprotinin [10 μg/ml], leupeptin [10 μg/ml], 1 mM phenylmethylsulfonyl fluoride) to
257 prepare whole-cell extracts. Lysates were cleared by centrifugation at 20,400 × g for 15
258 min at 4 °C. The clarified supernatants were subjected to affinity purification with anti-
259 FLAG (M2)–agarose affinity gel (Sigma-Aldrich), and then proteins eluted with FLAG
260 peptide (Sigma-Aldrich) was separated by SDS-PAGE and stained with silver. The
261 stained gels were sliced into pieces, and the abundant proteins therein were subjected to
262 in-gel digestion with trypsin. The resulting peptides were dried, dissolved in a mixture of
263 0.1% trifluoroacetic acid and 2% acetonitrile, and then applied to a nanoflow LC system
264 (Advanced UHPLC; Michrom BioResources, Auburn, CA, USA) equipped with an L-
265 column (C18, 0.15 by 50 mm, particle size of 3 μm; CERI, Tokyo, Japan). LC–MS/MS
266 analysis was performed with an Orbitrap Velos Pro instrument (Thermo Fisher Scientific).

267 All MS/MS spectra were compared with protein sequences in the International Protein
268 Index (IPI, European Bioinformatics Institute) mouse version 3.44 with the use of the
269 MASCOT algorithm. Assigned high-scoring peptide sequences were considered for
270 correct identification. Identified peptides from 3 independent experiments were integrated
271 and regrouped by IPI accession number. Proteins detected in ≥2 of 3 independent
272 experiments from FLAG-PDZD8–expressing cells, but absent from control cells, were
273 considered PDZD8-associated. Semi-quantitative abundance was estimated from
274 identification frequency (IF; number of identified peptides per protein normalized to the
275 number of theoretically detectable tryptic peptides). Functional categorization of
276 PDZD8-associated proteins was categorized with use of the UniProtKB database
277 (https://www.uniprot.org) based on Gene Ontology (GO) annotations. The proteins listed
278 in figure 1a shows endosome-related (GO:0005768), as well as columns for lysosome
279 (GO:0005764) or cholesterol-related as well.
280
281 **RNA interference, reverse transcription, and real-time PCR analysis**
282 Stealth siRNAs targeted to human TMEM55B (siTMEM55B#1, 5'-
283 ACGUGGAAGGCAAGAUGCAUCAGCA-3'; siTMEM55B#2, 5'-
284 CAAGAUGCAUCAGCAUGUAGUCAAA-3'), rat TMEM55B (siTMEM55B#1, 5'-
285 UGCUGAUGCAUCUUGCCUUCCACGU-3'; siTMEM55B#2, 5'-
286 CAAGAUGCAUCAGCAUGUAGUCAAA-3'), and non-targeting control were obtained
287 from Invitrogen Life Technologies. (Invitrogen Life Technologies, Carlsbad, CA, USA).
288 Human siRNAs were introduced into HeLa cells with the use of Lipofectamine
289 RNAiMAX (Invitrogen Life Technologies), and rat siRNAs were introduced into PC12
290 cells with the use of a Cell Line Nucleofector Kit V (VCA-1003) and Nucleofector
291 instrument (Lonza, Basel, Switzerland) according to the manufacturer's protocol. The
292 cells were then cultured for 48 h (for HeLa) or 72 h (for PC12). Total RNA was isolated
293 from cells with the use of an RNeasy Mini Kit (Qiagen, Hilden, Germany) according to
294 the manufacturer's protocol and was subjected to reverse transcription (RT) with the use
295 of a QuantiTect Rev Transcription Kit (Qiagen). The resulting cDNA was subjected to
296 real-time PCR analysis with Power SYBR Green PCR Master Mix in an ABI-Prism 7000
297 sequence detection system (Applied Biosystems, Foster City, CA). The amounts of each
298 target mRNA were calculated and normalized by that of GAPDH mRNA. Primers for
299 PCR (forward and reverse, respectively) were as follows: 5'-
300 GTCAGTGGTGGACCTGACCTG-3' and 5'-AAAGTGGTCGTTGAGGGCAAT-3' for
301 human GAPDH; 5'-CGAGTCTGCCAATCTCTCATC-3' and 5'-
302 AGTGCGGTCTGTGAACTCTGT-3' for human TMEM55B; 5'-

303 AAGGCTGAGAATGGGAAGCTG-3' and 5'-GGAGATGATGACCCTTTTGGC-3' for
304 rat GAPDH; 5'-CTAGCCCGGATAGTGGGAGTG-3' and 5'-
305 TTCCTGGAGGTGCATTCTTGA-3' for rat TMEM55B.
306

307 **Fluorescence imaging of live cells**

308 LysoTracker Red DND-99 (0.2 μM) or LysoSensor Green DND-189 (0.2 μM) (Thermo
309 Fisher Scientific, Rockford, IL, USA) were added to cells for 1 h at 37 °C according to
310 the manufacturer's protocol. HeLa and PC12 cells expressing plasmid-encoded
311 fluorescent proteins for 24 h and 96 h respectively, or metabolically labeled with
312 fluorescent probes were observed with an LSM800 confocal microscope (Zeiss,
313 Oberkochen, Germany), and the images were processed for calculation of fluorescence
314 intensity with ZEN imaging software (Zeiss) as well as Fiji (ImageJ, https://fiji.sc).
315

316 **Ca^{2+} imaging**

317 Cell media of HeLa cells expressing organelle-targeted Ca^{2+} indicators were pre-
318 incubated with HEPES-buffered saline (HBS; 137 mM NaCl, 5.9 mM KCl, 2.2 mM $CaCl_2$,
319 1.2 mM $MgCl_2$, 10 mM HEPES, 14 mM glucose, pH 7.4) for 1 h at 37 °C and then
320 stimulated with ATP (200 μM) (Wako, Japan). The images were captured by Operetta
321 high-content screening system (PerkinElmer, Waltham, MA, USA) using a ×20 objective
322 (λ_ex 460–490 nm; λ_em 500–550 nm) at the time point of ATP addition (t = 0 s) and
323 continued time points (t = X s) at a rate of one frame per 20 sec for total 1240 sec (G-
324 CEPIA) or 180 sec (Ly-GG and CEPIA3mt). The concentration of Ca^{2+} for each time
325 points was calculated by $\Delta F/F_0 = (F_x - F_0)/F_0$. Images were analyzed by Harmony
326 software (PerkinElmer).
327

328 **Immunoblot analysis**

329 HeLa cells were lysed in Triton lysis buffer containing 40 mM HEPES-NaOH (pH 7.6),
330 150 mM NaCl, 0.5% Triton X-100, 10 mM $MgCl_2$, 1 mM Na_3VO_4, 25 mM NaF, 1 mM
331 EDTA, 1 mM PMSF, leupeptin (10 μg/mL), and 10% glycerol. After 10 min on ice,
332 lysates were centrifuged at 15,000 × g for 10 min at 4 °C, and protein concentrations were
333 determined with the Pierce BCA Protein Assay (Thermo Fisher Scientific). Extracts were
334 resolved by SDS–PAGE, transferred to Immobilon-P membranes (Merck Millipore,
335 Darmstadt, Germany), and probed with primary antibodies. Signals were developed with
336 SuperSignal reagents (Thermo Fisher Scientific) and imaged on an LAS-4000 (GE
337 Healthcare, Waukesha, WI, USA).
338

339 **Statistical analysis**

340 Statistical analyses were performed with BellCurve for Excel software (Social Survey
341 Research Information, Tokyo, Japan). Normality of data was assessed with the Shapiro–
342 Wilk test. If the normality assumption was not met, the Kruskal–Wallis test with the
343 Steel's multiple comparisons test were applied. If data were normally distributed, One-
344 way repeated-measures analysis of variance (ANOVA) with the Dunnett's multiple
345 comparisons test were performed. Quantitative data are presented as mean ± SE.
346 Statistical significance of a *P* value is indicated as $0.01 \leq p < 0.05$ (*); $0.001 \leq p < 0.01$
347 (**); $p < 0.001$ (***); $p \geq 0.05$ (n.s.). Sample size (*n*) are in the figure legends.
348

349 **References**

350 1 Luo, J., Jiang, L. Y., Yang, H. & Song, B. L. Intracellular Cholesterol Transport
351 by Sterol Transfer Proteins at Membrane Contact Sites. *Trends Biochem Sci* **44**,
352 273-292, doi:10.1016/j.tibs.2018.10.001 (2019).
353 2 Wong, L. H., Gatta, A. T. & Levine, T. P. Lipid transfer proteins: the lipid
354 commute via shuttles, bridges and tubes. *Nat Rev Mol Cell Biol* **20**, 85-101,
355 doi:10.1038/s41580-018-0071-5 (2019).
356 3 Shirane, M. Lipid Transfer-Dependent Endosome Maturation Mediated by
357 Protrudin and PDZD8 in Neurons. *Front Cell Dev Biol* **8**, 615600,
358 doi:10.3389/fcell.2020.615600 (2020).
359 4 van der Kant, R. & Neefjes, J. Small regulators, major consequences - Ca(2)(+)
360 and cholesterol at the endosome-ER interface. *J Cell Sci* **127**, 929-938,
361 doi:10.1242/jcs.137539 (2014).
362 5 Ikonen, E. Cellular cholesterol trafficking and compartmentalization. *Nat Rev*
363 *Mol Cell Biol* **9**, 125-138, doi:10.1038/nrm2336 (2008).
364 6 Goldstein, J. L. & Brown, M. S. A century of cholesterol and coronaries: from
365 plaques to genes to statins. *Cell* **161**, 161-172, doi:10.1016/j.cell.2015.01.036
366 (2015).
367 7 Luo, J., Yang, H. & Song, B. L. Mechanisms and regulation of cholesterol
368 homeostasis. *Nat Rev Mol Cell Biol* **21**, 225-245, doi:10.1038/s41580-019-0190-
369 7 (2020).
370 8 Mehta, N. *et al.* The evolving role of cholesteryl ester transfer protein inhibition
371 beyond cardiovascular disease. *Pharmacol Res* **197**, 106972,
372 doi:10.1016/j.phrs.2023.106972 (2023).

9 Martin, M. G., Pfrieger, F. & Dotti, C. G. Cholesterol in brain disease: sometimes determinant and frequently implicated. *EMBO Rep* **15**, 1036-1052, doi:10.15252/embr.201439225 (2014).

10 Zechner, R., Madeo, F. & Kratky, D. Cytosolic lipolysis and lipophagy: two sides of the same coin. *Nat Rev Mol Cell Biol* **18**, 671-684, doi:10.1038/nrm.2017.76 (2017).

11 Schuck, S. Microautophagy - distinct molecular mechanisms handle cargoes of many sizes. *J Cell Sci* **133**, doi:10.1242/jcs.246322 (2020).

12 Haidar, M., Loix, M., Bogie, J. F. J. & Hendriks, J. J. A. Lipophagy: a new player in CNS disorders. *Trends Endocrinol Metab* **32**, 941-951, doi:10.1016/j.tem.2021.08.010 (2021).

13 Lan, Z. Q., Ge, Z. Y., Lv, S. K., Zhao, B. & Li, C. X. The regulatory role of lipophagy in central nervous system diseases. *Cell Death Discov* **9**, 229, doi:10.1038/s41420-023-01504-z (2023).

14 Shirane, M. & Nakayama, K. I. Protrudin induces neurite formation by directional membrane trafficking. *Science* **314**, 818-821, doi:10.1126/science.1134027 (2006).

15 Guillen-Samander, A., Bian, X. & De Camilli, P. PDZD8 mediates a Rab7-dependent interaction of the ER with late endosomes and lysosomes. *Proc Natl Acad Sci U S A* **116**, 22619-22623, doi:10.1073/pnas.1913509116 (2019).

16 Shirane, M. *et al.* Protrudin and PDZD8 contribute to neuronal integrity by promoting lipid extraction required for endosome maturation. *Nat Commun* **11**, 4576, doi:10.1038/s41467-020-18413-9 (2020).

17 Elbaz-Alon, Y. *et al.* PDZD8 interacts with Protrudin and Rab7 at ER-late endosome membrane contact sites associated with mitochondria. *Nat Commun* **11**, 3645, doi:10.1038/s41467-020-17451-7 (2020).

18 Khan, H., Chen, L., Tan, L. & Im, Y. J. Structural basis of human PDZD8-Rab7 interaction for the ER-late endosome tethering. *Sci Rep* **11**, 18859, doi:10.1038/s41598-021-98419-5 (2021).

19 Gao, Y., Xiong, J., Chu, Q. Z. & Ji, W. K. PDZD8-mediated lipid transfer at contacts between the ER and late endosomes/lysosomes is required for neurite outgrowth. *J Cell Sci* **135**, doi:10.1242/jcs.255026 (2022).

20 Thakur, R. S. & O'Connor-Giles, K. M. PDZD8 promotes autophagy at ER-lysosome membrane contact sites to regulate activity-dependent synaptic growth. *Cell Rep* **44**, 115483, doi:10.1016/j.celrep.2025.115483 (2025).

408 21 Alva, V. & Lupas, A. N. The TULIP superfamily of eukaryotic lipid-binding
409 proteins as a mediator of lipid sensing and transport. *Biochim Biophys Acta*
410 **1861**, 913-923, doi:10.1016/j.bbalip.2016.01.016 (2016).
411 22 Wong, L. H. & Levine, T. P. Tubular lipid binding proteins (TULIPs) growing
412 everywhere. *Biochim Biophys Acta Mol Cell Res* **1864**, 1439-1449,
413 doi:10.1016/j.bbamcr.2017.05.019 (2017).
414 23 Morita, K. *et al.* PDZD8-deficient mice accumulate cholesteryl esters in the
415 brain as a result of impaired lipophagy. *iScience* **25**, 105612,
416 doi:10.1016/j.isci.2022.105612 (2022).
417 24 Al-Amri, A. H. *et al.* PDZD8 Disruption Causes Cognitive Impairment in
418 Humans, Mice, and Fruit Flies. *Biol Psychiatry* **92**, 323-334,
419 doi:10.1016/j.biopsych.2021.12.017 (2022).
420 25 Kurihara, Y. *et al.* PDZD8-deficient mice manifest behavioral abnormalities
421 related to emotion, cognition, and adaptation due to dyslipidemia in the brain.
422 *Mol Brain* **16**, 11, doi:10.1186/s13041-023-01002-4 (2023).
423 26 Chan, R. B. *et al.* Comparative lipidomic analysis of mouse and human brain
424 with Alzheimer disease. *J Biol Chem* **287**, 2678-2688,
425 doi:10.1074/jbc.M111.274142 (2012).
426 27 van der Kant, R. *et al.* Cholesterol Metabolism Is a Druggable Axis that
427 Independently Regulates Tau and Amyloid-beta in iPSC-Derived Alzheimer's
428 Disease Neurons. *Cell Stem Cell* **24**, 363-375 e369,
429 doi:10.1016/j.stem.2018.12.013 (2019).
430 28 Nugent, A. A. *et al.* TREM2 Regulates Microglial Cholesterol Metabolism upon
431 Chronic Phagocytic Challenge. *Neuron* **105**, 837-854 e839,
432 doi:10.1016/j.neuron.2019.12.007 (2020).
433 29 Blanchard, J. W. *et al.* APOE4 impairs myelination via cholesterol dysregulation
434 in oligodendrocytes. *Nature* **611**, 769-779, doi:10.1038/s41586-022-05439-w
435 (2022).
436 30 Guo, J. L. *et al.* Decreased lipidated ApoE-receptor interactions confer
437 protection against pathogenicity of ApoE and its lipid cargoes in lysosomes. *Cell*
438 **188**, 187-206 e126, doi:10.1016/j.cell.2024.10.027 (2025).
439 31 Mayran, N., Parton, R. G. & Gruenberg, J. Annexin II regulates multivesicular
440 endosome biogenesis in the degradation pathway of animal cells. *EMBO J* **22**,
441 3242-3253, doi:10.1093/emboj/cdg321 (2003).

32 Lloyd-Evans, E. *et al.* Niemann-Pick disease type C1 is a sphingosine storage disease that causes deregulation of lysosomal calcium. *Nat Med* **14**, 1247-1255, doi:10.1038/nm.1876 (2008).

33 Bissig, C. *et al.* Viral infection controlled by a calcium-dependent lipid-binding module in ALIX. *Dev Cell* **25**, 364-373, doi:10.1016/j.devcel.2013.04.003 (2013).

34 Bretou, M. *et al.* Accumulation of APP C-terminal fragments causes endolysosomal dysfunction through the dysregulation of late endosome to lysosome-ER contact sites. *Dev Cell* **59**, 1571-1592 e1579, doi:10.1016/j.devcel.2024.03.030 (2024).

35 Churchill, G. C. *et al.* NAADP mobilizes Ca(2+) from reserve granules, lysosome-related organelles, in sea urchin eggs. *Cell* **111**, 703-708, doi:10.1016/s0092-8674(02)01082-6 (2002).

36 Calcraft, P. J. *et al.* NAADP mobilizes calcium from acidic organelles through two-pore channels. *Nature* **459**, 596-600, doi:10.1038/nature08030 (2009).

37 Galione, A. A primer of NAADP-mediated Ca(2+) signalling: From sea urchin eggs to mammalian cells. *Cell Calcium* **58**, 27-47, doi:10.1016/j.ceca.2014.09.010 (2015).

38 Kilpatrick, B. S. *et al.* An Endosomal NAADP-Sensitive Two-Pore Ca(2+) Channel Regulates ER-Endosome Membrane Contact Sites to Control Growth Factor Signaling. *Cell Rep* **18**, 1636-1645, doi:10.1016/j.celrep.2017.01.052 (2017).

39 Yuan, Y. *et al.* Two-pore channel-2 and inositol trisphosphate receptors coordinate Ca(2+) signals between lysosomes and the endoplasmic reticulum. *Cell Rep* **43**, 113628, doi:10.1016/j.celrep.2023.113628 (2024).

40 Zheng, Q. *et al.* Calcium transients on the ER surface trigger liquid-liquid phase separation of FIP200 to specify autophagosome initiation sites. *Cell* **185**, 4082-4098 e4022, doi:10.1016/j.cell.2022.09.001 (2022).

41 Ungewickell, A. *et al.* The identification and characterization of two phosphatidylinositol-4,5-bisphosphate 4-phosphatases. *Proc Natl Acad Sci U S A* **102**, 18854-18859, doi:10.1073/pnas.0509740102 (2005).

42 Zou, J., Marjanovic, J., Kisseleva, M. V., Wilson, M. & Majerus, P. W. Type I phosphatidylinositol-4,5-bisphosphate 4-phosphatase regulates stress-induced apoptosis. *Proc Natl Acad Sci U S A* **104**, 16834-16839, doi:10.1073/pnas.0708189104 (2007).

477 43 Hashimoto, Y., Shirane, M. & Nakayama, K. I. TMEM55B contributes to
478 lysosomal homeostasis and amino acid-induced mTORC1 activation. *Genes*
479 *Cells* **23**, 418-434, doi:10.1111/gtc.12583 (2018).
480 44 Xu, H. & Ren, D. Lysosomal physiology. *Annu Rev Physiol* **77**, 57-80,
481 doi:10.1146/annurev-physiol-021014-071649 (2015).
482 45 Banerjee, S. & Kane, P. M. Regulation of V-ATPase Activity and Organelle pH
483 by Phosphatidylinositol Phosphate Lipids. *Front Cell Dev Biol* **8**, 510,
484 doi:10.3389/fcell.2020.00510 (2020).
485 46 Ballabio, A. & Bonifacino, J. S. Lysosomes as dynamic regulators of cell and
486 organismal homeostasis. *Nat Rev Mol Cell Biol* **21**, 101-118,
487 doi:10.1038/s41580-019-0185-4 (2020).
488 47 Willett, R. *et al.* TFEB regulates lysosomal positioning by modulating
489 TMEM55B expression and JIP4 recruitment to lysosomes. *Nat Commun* **8**,
490 1580, doi:10.1038/s41467-017-01871-z (2017).
491 48 Jeong, E., Willett, R., Rissone, A., La Spina, M. & Puertollano, R. TMEM55B
492 links autophagy flux, lysosomal repair, and TFE3 activation in response to
493 oxidative stress. *Nat Commun* **15**, 93, doi:10.1038/s41467-023-44316-6 (2024).
494 49 Medina, M. W. *et al.* Transmembrane protein 55B is a novel regulator of cellular
495 cholesterol metabolism. *Arterioscler Thromb Vasc Biol* **34**, 1917-1923,
496 doi:10.1161/ATVBAHA.113.302806 (2014).
497 50 Qin, Y. *et al.* Phosphatidylinositol-(4,5)-Bisphosphate Regulates Plasma
498 Cholesterol Through LDL (Low-Density Lipoprotein) Receptor Lysosomal
499 Degradation. *Arterioscler Thromb Vasc Biol* **40**, 1311-1324,
500 doi:10.1161/ATVBAHA.120.314033 (2020).
501 51 Matsumoto, M. *et al.* Large-scale proteomic analysis of tyrosine-
502 phosphorylation induced by T-cell receptor or B-cell receptor activation reveals
503 new signaling pathways. *Proteomics* **9**, 3549-3563,
504 doi:10.1002/pmic.200900011 (2009).
505 52 Kakimoto, Y. *et al.* Visualizing multiple inter-organelle contact sites using the
506 organelle-targeted split-GFP system. *Sci Rep* **8**, 6175, doi:10.1038/s41598-018-
507 24466-0 (2018).
508 53 Suzuki, J. *et al.* Imaging intraorganellar Ca2+ at subcellular resolution using
509 CEPIA. *Nat Commun* **5**, 4153, doi:10.1038/ncomms5153 (2014).
510 54 Atakpa, P., Thillaiappan, N. B., Mataragka, S., Prole, D. L. & Taylor, C. W.
511 IP(3) Receptors Preferentially Associate with ER-Lysosome Contact Sites and

Selectively Deliver Ca(2+) to Lysosomes. *Cell Rep* **25**, 3180-3193 e3187, doi:10.1016/j.celrep.2018.11.064 (2018).

55 Otera, H. *et al.* A novel insertion pathway of mitochondrial outer membrane proteins with multiple transmembrane segments. *J Cell Biol* **179**, 1355-1363, doi:10.1083/jcb.200702143 (2007).

Acknowledgements and Funding Information

We thank Y. Tamura for split-GFP cDNAs; E. Taylor for Ly-GG cDNA; K. Mihara for Su9 cDNA; K. I. Nakayama and T. Ohnishi for proteome analysis; K. Sato and K. Kato for Ca^{2+} imaging analysis; and the Research Equipment Sharing Center at Nagoya City University for assistance. This work was supported in part by KAKENHI grants from Japan Society for the Promotion of Science (JSPS) to M.S. (24K02122).

Author contributions statement

M.S. designed experiments, supervised the study, analyzed the data, and wrote the manuscript. N.M. and H.M. performed experiments.

Additional information

Data availability

The MS data have been deposited in the JPOST Repository Database as follows:
URL: https://repository.jpostdb.org
JPID and PXID are as follows;
Mock-FLAG complex in Neuro2A; (1) JPST004039, PXD067776; (2) JPST004040, PXD067777; (3) JPST004041, PXD067779.
PDZD8-FLAG complex in Neuro2A; (1) JPST004042, PXD067780; (2) JPST004043, PXD067782; (3) JPST004044, PXD067783.

Supplementary datasets

Raw data is provided within the supplementary information files.

Competing interests

The authors declare no competing interests.

Correspondence

Correspondence and requests for materials should be addressed to M.S. (shiram@phar.nagoya-cu.ac.jp)

548
549

550 **Figure Legends**

551 **Fig. 1.** Identification of PDZD8-associated proteins by proteomic analysis. (**A**)
552 Endosome-related proteins identified as PDZD8-associated proteins. Protein abundance
553 was estimated semiquantitatively by identification frequency (IF). Asterisks indicate
554 proteins previously reported as TMEM55B-associated. Lysosome (Ly)-localized and
555 cholesterol (Chol)-related proteins are also indicated. Proteins were categorized based on
556 Gene Ontology (GO) terms and UniProtKB annotations. (**B, C**) HeLa cells were
557 transfected with siControl, siTMEM55B#1, or siTMEM55B#2. Total RNA was analyzed
558 by RT-qPCR for TMEM55B mRNA (B), and protein levels were examined by
559 immunoblotting with anti-TMEM55B and anti-HSP90 antibodies (C). Data are shown as
560 mean ± SE (n = 9 for RNA analysis). ***$p < 0.001$ (one-way ANOVA with Dunnett's
561 multiple comparisons). (**D**) HeLa cells were transfected with siControl, siTMEM55B#1,
562 or siTMEM55B#2 together with split-GFP vectors ERj1–GFP(1–10) and LAMP1–
563 GFP(11), along with mCherry as a transfection control. Scale bar, 10 µm. (**E**)
564 Quantification of split-GFP fluorescence normalized to mCherry intensity as in (D). n =
565 38, 36, and 37 cells for siControl, siTMEM55B#1, and siTMEM55B#2, respectively. n.s.,
566 not significant (Kruskal–Wallis test with Steel's multiple comparisons).
567

568 **Fig. 2.** TMEM55B depletion impairs lysosomal acidification and lipolysis. (**A, C**) HeLa
569 cells transfected with siControl, siTMEM55B#1, or siTMEM55B#2 were stained with
570 LysoTracker Red (A) or LysoSensor Green (C) and analyzed by confocal microscopy.
571 Boxed areas (top panels) are shown at higher magnification (bottom panels). Scale bars,
572 10 µm (top and middle) and 5 µm (bottom). (**B, D**) Quantification of LysoTracker Red
573 (B) or LysoSensor Green (D) mean fluorescence intensity per lysosome in (A) (n = 746,
574 497, and 452 lysosomes for siControl, siTMEM55B#1, and siTMEM55B#2,
575 respectively) or (C) (n = 703, 847, and 794 lysosomes, respectively). (**E**) RT-qPCR
576 analysis of TMEM55B mRNA in PC12 cells transfected with siControl, siTMEM55B#1,
577 or siTMEM55B#2 (mean ± SE, n = 6). (**F**) PC12 cells were transfected with siControl,
578 siTMEM55B#1, or siTMEM55B#2 together with EGFP-PLIN2, and stained with
579 LysoTracker Red. (**G**) Quantification of lipid droplet (LD) size (µm²) of EGFP-PLIN2
580 puncta in (F) (n = 627, 450, and 317 LDs for siControl, siTMEM55B#1, and
581 siTMEM55B#2, respectively). (**H**) Quantification of mean EGFP-PLIN2 fluorescence
582 intensity per cell in (F) (n = 52, 41, and 35 cells for siControl, siTMEM55B#1, and
583 siTMEM55B#2, respectively). (**I**) Quantification of mean LysoTracker Red fluorescence
584 intensity per cell in (F) (n = 52, 41, and 35 cells, respectively). (**J**) Pearson's correlation
585 coefficient between EGFP-PLIN2 and LysoTracker Red per cell in (F) (n = 52, 41, and

586 35 cells, respectively). ***p < 0.001, **p < 0.01 (Kruskal–Wallis test with Steel's
587 multiple comparisons test in B, D, and G–I); **p < 0.01, *p < 0.05 (one-way ANOVA
588 with Dunnett's multiple comparisons in E and J).
589
590 **Fig. 3.** Depletion of TMEM55B impairs Ca^{2+} release from the ER. (**A**) Schematic
591 representation of G-CEPIA1er, a Ca^{2+} indicator with the G-GECO1 domain facing the
592 ER lumen. (**B**) Confocal images of HeLa cells co-expressing G-CEPIA1er (green) and
593 the ER marker mCherry-KDEL (red). Scale bar, 10 μm. (**C**) Time lapse analysis of G-
594 CEPIA1er fluorescence ($\Delta F/F_0$) in cells transfected with siControl (gray, n = 30 fields),
595 siTMEM55B#1 (red, n = 30), or siTMEM55B#2 (pink, n = 30). ATP (200 μM) was added
596 at t = 0 s; Data are mean ± SE. (**D**) Quantification of peak $\Delta F/F_0$ values in (C).
597 (**E**) Quantification of the slope of G-CEPIA1er $\Delta F/F_0$ during 0–120 s after ATP addition
598 ($\Delta F/F_0 \cdot s^{-1}$). (**F**) Quantification of time (s) to peak after ATP addition for G-CEPIA1er
599 $\Delta F/F_0$. (**G**) Quantification of the slope of G-CEPIA1er $\Delta F/F_0$ during 900 s after the peak
600 ($\Delta F/F_0 \cdot s^{-1}$). Data are mean ± SE; ***p < 0.001, *p < 0.05 (Kruskal–Wallis test with
601 Steel's multiple comparisons in D, F, and G); ***p < 0.001 (one-way ANOVA with
602 Dunnett's multiple comparisons in E).
603
604 **Fig. 4.** Depletion of TMEM55B impairs lysosomal Ca^{2+} dynamics. (**A**) Schematic
605 representation of Ly-GG, a Ca^{2+} indicator with the G-GECO1 domain facing the cytosolic
606 side of the lysosomal membrane. (**B**) Confocal images of HeLa cells co-expressing Ly-
607 GG (green) and the lysosomal marker mCherry–LAMP1 (red). Scale bar, 10 μm. (**C**)
608 Time lapse analysis of Ly-GG fluorescence ($\Delta F/F_0$) in cells transfected with siControl
609 (gray, n = 29 fields), siTMEM55B#1 (red, n = 29), or siTMEM55B#2 (pink, n = 26). ATP
610 (200 μM) was added at t = 0 s; Data are mean ± SE and normalized by subtracting values
611 from ATP-free cells, in which fluorescence declined due to photobleaching. (**D, E**)
612 Quantification of Ly-GG slopes during 0–60 s (D) and 60–160 s (E) ($\Delta F/F_0 \cdot s^{-1}$). (**F**)
613 Schematic representation of CEPIA3mt, a Ca^{2+} indicator with the GCaMP2 domain
614 facing the mitochondrial matrix. (**G**) Confocal images of HeLa cells co-expressing
615 CEPIA3mt (green) and the mitochondrial marker Su9–RFP (red). Scale bar, 10 μm. (**H**)
616 Time lapse analysis of CEPIA3mt fluorescence ($\Delta F/F_0$) in cells transfected with control
617 siRNA (gray, n = 25 fields), siTMEM55B#1 (red, n = 26), or siTMEM55B#2 (pink, n =
618 24). ATP (200 μM) was added at t = 0 s; Data are mean ± SE. (**I, J**) Quantification of
619 CEPIA3mt slopes during 0–60 s (I) and 60–160 s (J) ($\Delta F/F_0 \cdot s^{-1}$). Data are mean ± SE;
620 ***p < 0.001; (Kruskal–Wallis test with Steel's multiple comparisons in D and E); n.s.,
621 not significant (one-way ANOVA with Dunnett's multiple comparisons in I and J).

622

623 **Fig. 5.** Model of the mechanism where TMEM55B promotes lipolysis via lysosomal
624 acidification and calcium regulation at ER-Ly MCSs. ER protein PDZD8 is associated
625 with lysosome protein TMEM55B that promotes lysosomal acidification through
626 regulation of v-ATPase. Lysosomal acidification then promotes activity of lysosomal
627 acidic lipases that promote lipolysis and subsequently degradation of CEs to cholesterol,
628 as well as calcium channels that promote CICR. CICR at ER-Ly MCSs may also
629 contribute to lipolysis by fusion of LDs or LPs with lysosomes. ER, endoplasmic
630 reticulum; MCS, membrane contact site; v-ATPase, vacuolar-ATPase; TPC2, two-pore
631 channel 2; TRPML1, transient receptor potential mucolipin 1; RyR, ryanodine receptor;
632 IP_3R, inositol 1,4,5-trisphosphate receptor; CICR, Ca^{2+}-induced Ca^{2+} release; LD, lipid
633 droplet; LP, lipoprotein; CE, cholesteryl ester; Chol, cholesterol.
634

A

Gene symbol	Protein name	IF	Ly	Chol
Zfyve27	ISOFORM 1 OF ZINC FINGER FYVE DOMAIN-CONTAINING PROTEIN 27.	1.095		
Stmn2	STATHMIN-2.	0.500		
Vac14	PROTEIN VAC14 HOMOLOG.	0.324		
**Atp6v0d1*	VACUOLAR PROTON PUMP SUBUNIT D 1.	0.200	✓	
Sh3gl1	ENDOPHILIN-A2.	0.125		
Gm364	SIMILAR TO TRANSMEMBRANE 9 SUPERFAMILY MEMBER 2.	0.111		
**Lamtor1*	UPF0404 PROTEIN C11ORF59 HOMOLOG.	0.111	✓	✓
Tfrc	TRANSFERRIN RECEPTOR PROTEIN 1.	0.100		
**Tmem55b*	TRANSMEMBRANE PROTEIN 55B.	0.083	✓	✓
Fig4	SAC DOMAIN-CONTAINING PROTEIN 3.	0.048		
Sun2	PROEIN UNC-84 HOMOLOG B.	0.032		
Vps35	VACUOLAR PROTEIN SORTING-ASSOCIATED PROTEIN 35.	0.026	✓	
Kif13a	KINESIN-LIKE PROTEIN KIF13A.	0.014		

B

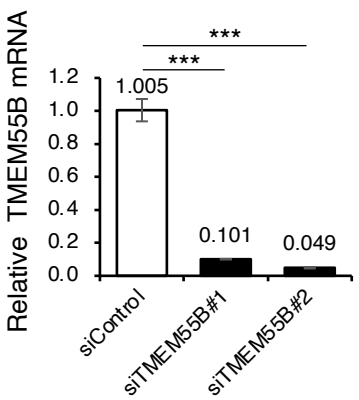

C

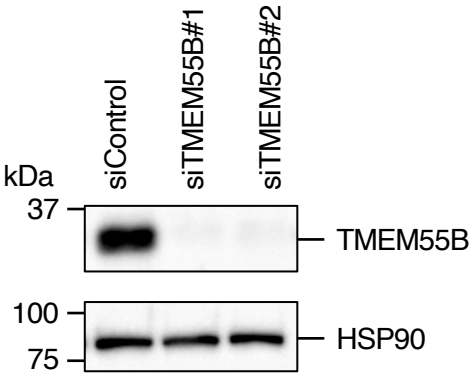

D

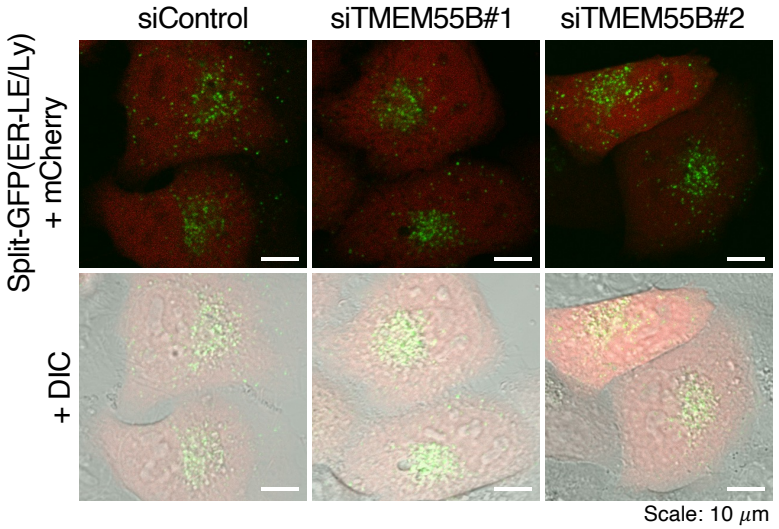

E

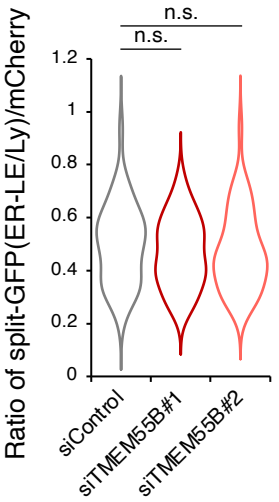

Figure 1

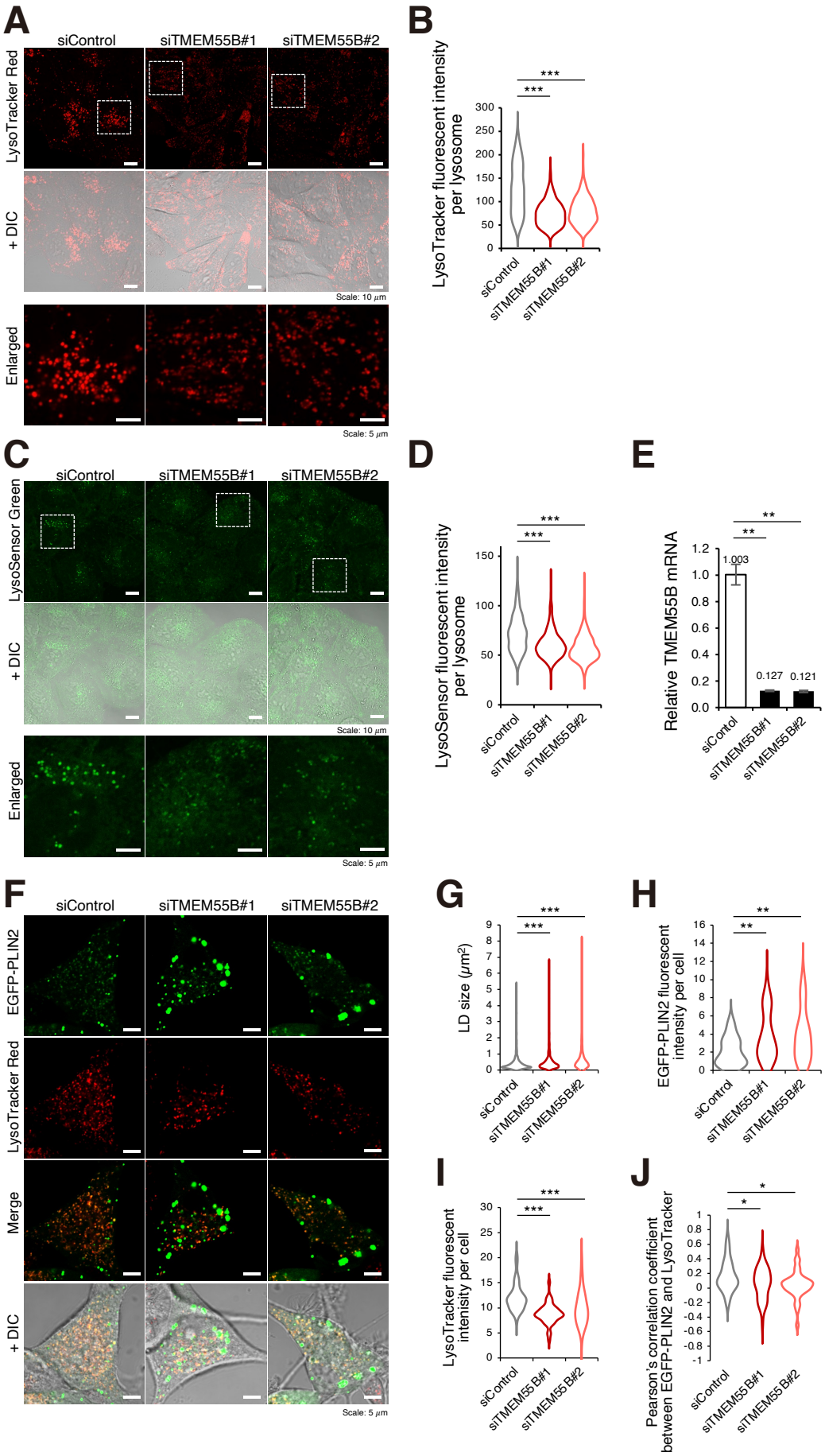
A
siControl
siTMEM55B#1
siTMEM55B#2
LysoTracker Red
+ DIC
Enlarged
Scale: 10 μm
Scale: 5 μm
B
LysoTracker fluorescent intensity per lysosome
***
***
siControl
siTMEM55B#1
siTMEM55B#2
C
LysoSensor Green
D
LysoSensor fluorescent intensity per lysosome
E
Relative TMEM55B mRNA
1.003
0.127
0.121
**
F
EGFP-PLIN2
Merge
G
LD size (μm²)
H
EGFP-PLIN2 fluorescent intensity per cell
I
LysoTracker fluorescent intensity per cell
J
Pearson's correlation coefficient between EGFP-PLIN2 and LysoTracker
*

Figure 2

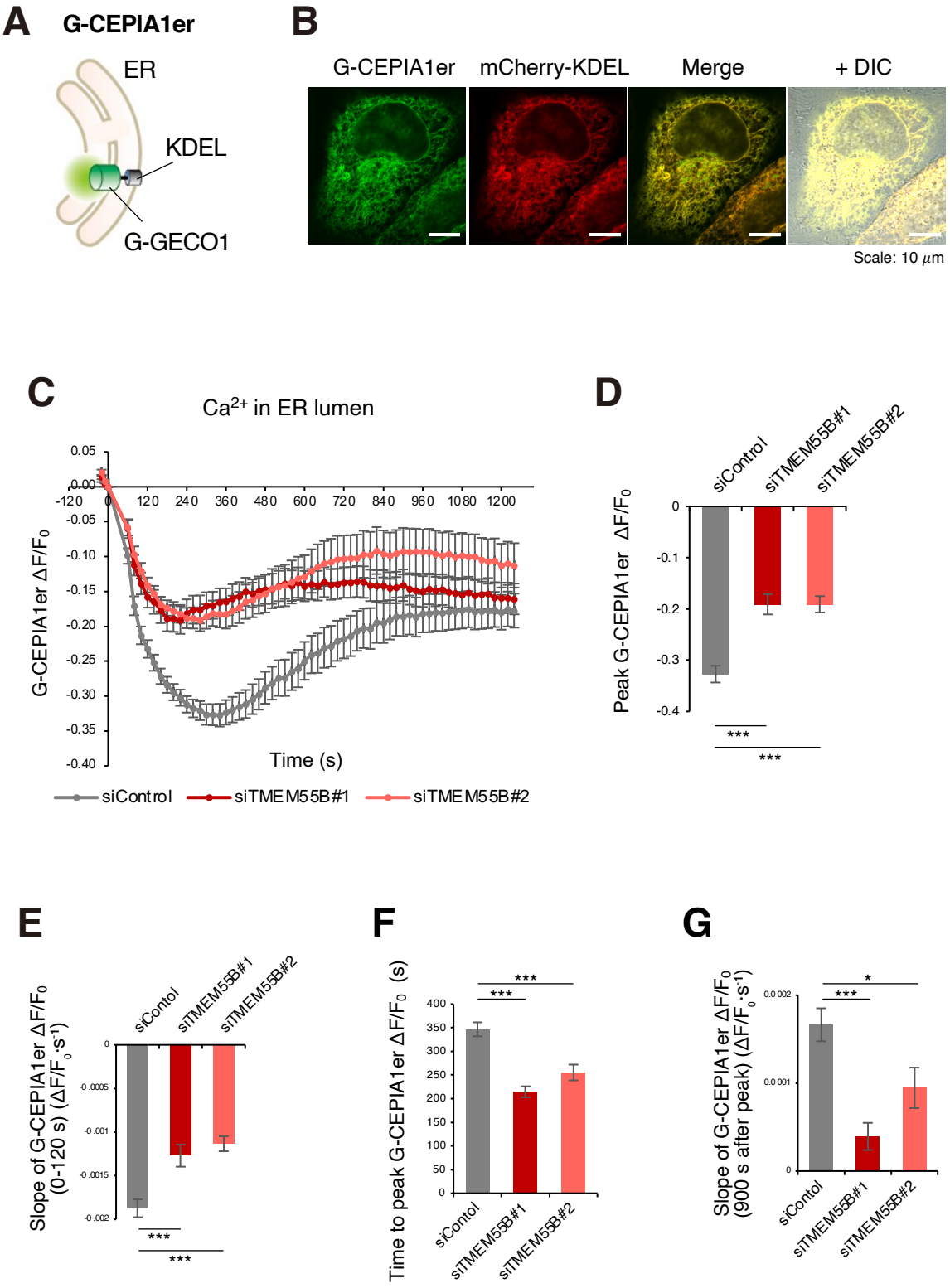
A
G-CEPIA1er
ER
KDEL
G-GECO1
B
G-CEPIA1er
mCherry-KDEL
Merge
+ DIC
Scale: 10 μm
C
Ca2+ in ER lumen
G-CEPIA1er ΔF/F0
Time (s)
siControl
siTMEM55B#1
siTMEM55B#2
D
Peak G-CEPIA1er ΔF/F0
siControl
siTMEM55B#1
siTMEM55B#2
***
***
E
Slope of G-CEPIA1er ΔF/F0 (0-120 s) (ΔF/F0·s-1)
siContol
siTMEM55B#1
siTMEM55B#2
***
***
F
Time to peak G-CEPIA1er ΔF/F0 (s)
siContol
siTMEM55B#1
siTMEM55B#2
***
***
G
Slope of G-CEPIA1er ΔF/F0 (900 s after peak) (ΔF/F0·s-1)
siContol
siTMEM55B#1
siTMEM55B#2
*
***

Figure 3

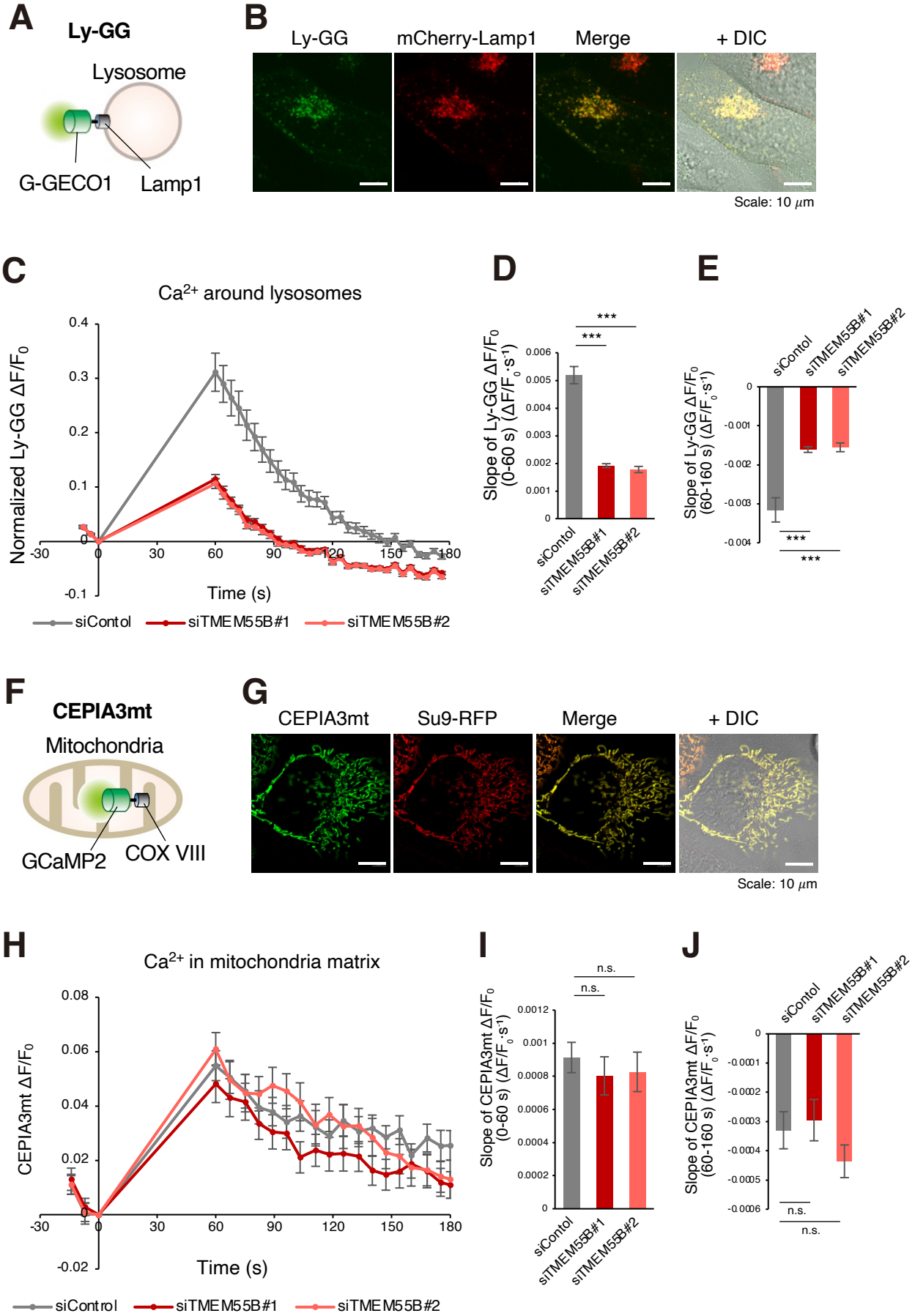
A
Ly-GG
Lysosome
G-GECO1
Lamp1
B
Ly-GG
mCherry-Lamp1
Merge
+ DIC
Scale: 10 μm
C
Ca2+ around lysosomes
Normalized Ly-GG ΔF/F0
Time (s)
siContol
siTMEM55B#1
siTMEM55B#2
D
Slope of Ly-GG ΔF/F0 (0-60 s) (ΔF/F0·s-1)
***
***
siContol
siTMEM55B#1
siTMEM55B#2
E
Slope of Ly-GG ΔF/F0 (60-160 s) (ΔF/F0·s-1)
siContol
siTMEM55B#1
siTMEM55B#2
***
***
F
CEPIA3mt
Mitochondria
GCaMP2
COX VIII
G
CEPIA3mt
Su9-RFP
Merge
+ DIC
Scale: 10 μm
H
Ca2+ in mitochondria matrix
CEPIA3mt ΔF/F0
Time (s)
siControl
siTMEM55B#1
siTMEM55B#2
I
Slope of CEPIA3mt ΔF/F0 (0-60 s) (ΔF/F0·s-1)
n.s.
n.s.
siContol
siTMEM55B#1
siTMEM55B#2
J
Slope of CEPIA3mt ΔF/F0 (60-160 s) (ΔF/F0·s-1)
siContol
siTMEM55B#1
siTMEM55B#2
n.s.
n.s.

Figure 4

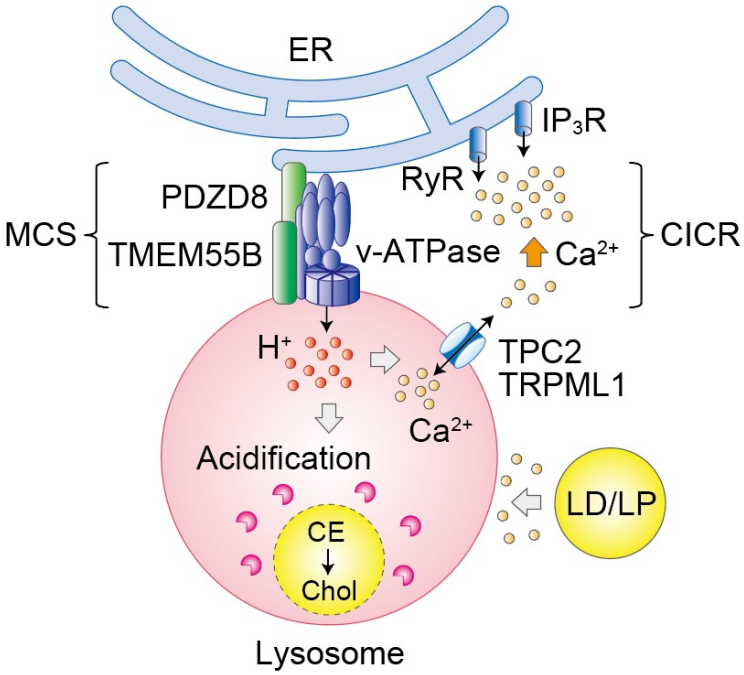
ER
IP3R
RyR
PDZD8
MCS
TMEM55B
v-ATPase
Ca2+
CICR
H+
TPC2
TRPML1
Ca2+
Acidification
LD/LP
CE
Chol
Lysosome

Figure 5